coatings

MDPI

Article

Temperature-Induced Formation of Lubricous Oxides in Vanadium Containing Iron-Based Arc Sprayed Coatings

Wolfgang Tillmann [1], Leif Hagen [1,*], David Kokalj [1], Michael Paulus [2] and Metin Tolan [2]

[1] Institute of Materials Engineering, TU Dortmund University, 44227 Dortmund, Germany; wolfgang.tillmann@tu-dortmund.de (W.T.); david.kokalj@tu-dortmund.de (D.K.)
[2] Fakultät Physik/DELTA, TU Dortmund University, 44227 Dortmund, Germany; michael.paulus@tu-dortmund.de (M.P.); metin.tolan@tu-dortmund.de (M.T.)
* Correspondence: leif.hagen@tu-dortmund.de; Tel.: +49-231-755-5715

Received: 12 November 2018; Accepted: 27 December 2018; Published: 29 December 2018

Abstract: In the field of surface engineering, the use of self-lubricous coatings with the incorporation of vanadium represent a promising approach to reduce friction, thus contributing to the wear behavior. For vanadium containing hard coatings produced by means of thin film technology, the reduction in friction at elevated temperatures was repeatedly attributed to temperature-induced and tribo-oxidatively formed oxides which act as solid lubricant. Only very few studies focused on the tribological characteristics of vanadium containing arc sprayed coatings. In this study, the tribological characteristics of a vanadium containing iron-based arc sprayed deposit were investigated in dry sliding experiments under ambient conditions and different temperatures. Types of wear at the worn surfaces and counterparts were examined by means of electron microscopy and energy dispersive X-ray (EDX) spectroscopy. The speciation of vanadium in the superficial layer was determined using X-ray absorption near edge structure (XANES) spectroscopy. It was found that the vanadium-containing coating exhibited a distinctly reduction of the coefficient of friction above 450 °C which further decreased with increasing temperature. XANES spectroscopy indicated an increased oxidation state for the V component on the coating surface, suggesting the prevalence of specific vanadium oxides which promote a self-lubricating ability of the coating.

Keywords: wire arc spray; friction behavior; lubricous oxides; XANES spectroscopy

1. Introduction

Tribo-oxidation was validated for practical applications as a favorite mechanism for the development of dry running tribosystems [1]. Over the last decades, self-lubricious hard coatings evolved into a promising candidate to provide an improved friction behavior, which in turn contributes to the wear resistance [2]. In the field of thin film technology, a reduction in friction has been achieved, among others, by using V-containing coatings [3]. For V-containing coatings, temperature-induced and tribo-oxidatively formed, low shear strength oxides act as solid lubricants, thus determining the lubricating capacity of functional surfaces. The participation of V forms oxides of the homologous series V_nO_{2n-1} with $3 < n < 10$ between the end members V_2O and VO_2, and are so-called Magnéli phases [4,5]. In addition, V_nO_{2n+1} type phases exist, where VO_2 and V_2O_5 represent the end members [5]. Some V-oxides belong to another homology according to the formula $V_{2n}O_{5n-2}$ [6] and are named as Wadsley phases. In summary, a number of compounds in the V–O system can be formed including stoichiometric and substoichiometric oxides, where V is present in number of valence states [7]. The slip ability of oxygen deficient phases of V-oxides has been univocally associated as crystallographic

shear [8]. When compared to intrinsic solid lubricants such as MoS_2, where every second layer features a crystallographic slip ability, only few layers depending on the stoichiometry exhibits a crystallographic shear structure in Magnéli phases. Woydt et al. [9] therefore clarified that a univocal association between the lubricity and Magnéli phases is not always correct. Regarding the lubricity of Magnéli phases, they emphasized that the rheological process can be better described by plastic flow instead of crystallographic shear.

V-oxides or their derivatives can be deposited, on the one hand, as coatings using reactive physical vapor deposition techniques [10–12], hydrothermal synthesis [13], and atmospheric pressure chemical vapor deposition [14]. On the other hand, an established approach is to deposit hard and wear-resistant coatings with the incorporation of V. Thereby, V acts as an active element source for the formation for various oxides that are primarily caused by tribo-chemical reactions at elevated temperatures in ambient air. In that respect, a major objective has been focused on the development of hard coatings with the participation of V incorporated as a solid solution [15–18]. Further studies emphasized the technological relevance of multilayered coating systems consisting of alternating thin layers of VN and another hard coating [19–23]. Concerning the tribological characteristics, the aforementioned studies revealed that the reduce in friction was attributed to certain types of V-oxides. As recently discussed [24], the temperature-induced formation of V-oxides depends, inter alia, on the V content and chemical composition of the coating system. Due to its low decohesion energy [5], vanadium pentoxide represents a promising candidate for solid lubricants at elevated temperatures. Above its melting point of 678 °C [25], it also acts as liquid lubricant [2]. Kutschej et al. [26] pointed out that the transformation of vanadium pentoxide into lower oxidized V-oxides with higher melting points in turn limits the lubricating capacity.

To date, only few authors examined the tribo-mechanical properties of arc sprayed coatings using a V-containing feedstock. Deng et al. [27] investigated the abrasive wear behavior of arc sprayed stainless steel coatings which contain a certain amount of V. The incorporation of V was accomplished by the addition of ferrovanadium as filler material. The authors demonstrated an enhanced wear resistance against abrasion, among others, due to the addition of V, which was found to favor the formation of vanadium carbides. With regard to the tribological investigations, the friction behavior of the V-containing coating was not investigated at all.

In this study, an arc-sprayed V-containing iron based coating is subjected to elevated temperatures and tested tribologically in dry sliding experiments. To scrutinize the wear mechanism of the tribological stressed surfaces, the wear tracks and counterbodies are investigated by means of electron microscopy and EDX spectroscopy. To characterize the temperature-induced oxide formation, the oxidation state of the V component of the reactive layer at the surface is determined by using XANES spectroscopy.

2. Materials and Methods

Prior to the coating deposition, round steel specimens (1.1191, 40 mm × 6 mm) were grit blasted with corundum (grit size: 1180–1700 µm), and cleaned in an ultrasonic ethanol bath. A Fe-based cored wire which contains approximately 29.9 wt % of V served as feedstock. Within this study, the produced coating which was deposited with the V-containing Fe-based (Fe-29.91V-0.38Al-0.33Si-0.25Mn-0.07C wt %) cored wire was referred to as Fe-V. To investigate the effect of V on the temperature-induced and tribo-oxidatively promoted oxide formation, a corresponding V-free Fe-based coating was produced with the use of a low alloy steel in the form of a cored wire (Fe-0.25Mn-0.11Si-0.07C), and consequently served as reference. The chemical composition of the cored wires was provided by the manufacture (Durum Verschleissschutz, Willich, Germany), and calculated based on the results conducted by chemical analysis of the steel strip (Fe-based sheath) and optical emission spectrometry of the filler material (ferrovanadium, low-alloy steel powder).

To produce the arc sprayed coatings, the Smart Arc 350 PPG spraying system (Oerlikon Metco, Pfäffikon, Switzerland) with the spray torch equipped with a conventional front-end hardware

(high-profile centering post, No. PPG5I976; air cap body (fine), No. PPG51416 [28]) was utilized. The optimized spray parameter settings were used based on the findings in a previous study [29] using a statistical design of experiments and multi-criteria optimization by means of Derringer's desirability function. This approach has been taken in order to produce dense and smooth coatings with an almost defect-free microstructure. In that respect, compressed air was utilized as atomization gas by applying a gas pressure of 0.6 MPa. The voltage and current was set to 28 V, and 180 A. The deposits were applied using a constant spray distance of 95 mm. The gun velocity of the spray torch and the track pitch were set to 200 mm/s, and 5 mm. Two overruns were executed in order to generate an adequate coating thickness of 418 $\pm$ 34 µm.

To ensure functional integrity, the produced deposits were metallographically examined. Cross sections of coated samples were prepared by using silicon carbide grinding discs (grit size: P80, P180; P600, and P2500 according to FEPA [30]) and polishing cloths with a diamond suspension (abrasive particle size: 9, 6, 3 and 1 µm). The microstructural characteristics of the produced coatings were examined at cross sections using a field emission scanning electron microscope (FE-SEM) type JSM-7001F (JEOL (Germany) GmbH, Freising, Germany). EDX spectra were acquired with an energy dispersive X-ray spectroscopy detector (Oxford Instruments, Abingdon, UK) in conjunction with the FE-SEM. To determine the chemical composition, the EDX spectra were evaluated with the use of the INCA software (Oxford Instruments, Abingdon, UK).

Coated samples from the same batch were further investigated with respect to the tribo-mechanical properties. Prior to the tribo-mechanical testing, the surface of the coated samples was machined using a silicon carbide grinding disk (grit size: P4000), and polished utilizing polishing cloths with diamond suspension (abrasive particle size: 3 µm and $^1/_4$ µm). The tribological tests were performed using the high-temperature ball-on-disk (BOD) tribometer (CSM Instruments, Peseux, Switzerland) at room temperature (25 °C) and elevated temperatures (from 350 up to 750 °C in 100 °C steps). The experiments were conducted without lubricant supply. For the dry sliding experiments, an alumina ball with a diameter of 6 mm and a hardness of 2300 HV0.3 was used as counterbody. The velocity was kept constant at 40 cm/s, and the radius of the circular path was set to 10 mm. A sliding distance of 200 m, and a load of 5 N were applied. The coefficient of friction (COF) was obtained from the relationship of the measured tangential force and the applied normal force. The fluctuations of the tangential force during sliding were extracted and afterwards analyzed by Fast Fourier Transformation (FFT) using the data analysis and graphing software OriginPro (OriginLab Corporation, Northampton, MA, USA). In order to assess the wear behaviour of the tribological stressed surfaces, the worn surfaces as well as the alumina counterbodies were investigated by means of electron microscopy and EDX spectroscopy, as described previously. Vickers microhardness (MH) measurements were conducted on the coating surfaces after tribological testing using the hardness testing device M400 (Leco, Saint Joseph, MI, USA) with 300 g loads. To determine the MH, five residual indents were taken into account.

Due to the rapid solidification (about ~10^5 °C/s) [31] of molten spray particles, arc spraying has great potential for the production of amorphous coatings, as already demonstrated in [32,33] for Fe-based coatings. XANES spectroscopy is a well-established technique for examination of the chemical structure of amorphous materials. It offers a unique possibility to identify the local structural environment of the atomic species in a material of unknown composition. Some XANES features are sensitive to the local symmetry and oxidation state of the exciting atom. Within the scope of this study, the oxidation state of the reactive layer at the surface of the Fe-V coating was analyzed using XANES at beamline BL10 of the synchrotron light source DELTA (Dortmund electron accelerator) at the TU Dortmund. The XANES measurements were conducted at the V K-edge (5465 eV). The measuring range was set to 60 eV before the V K-edge (5465 eV), and up to 100 eV after the K-edge. A step size of 2 eV was chosen before the K-edge, whereas the measurement was performed using a step size of 0.5 eV in the region of the K-edge in order to get an adequate resolution. After the K-edge the step size was set to 1 eV. A measurement time of 5 s per step was used. A silicon (111) channel-cut crystal served as a monochromator. The beam was set to 1 mm in height and 4 mm

in width. The angle of incidence was 5.0°, and the detection of the absorption was carried out by fluorescence. Different V-oxides (MaTeck, Jülich, Germany) were utilized for the XANES spectroscopy and served as reference for further examinations of the Fe-V coating. A V-foil (space group Im-3m, body-centered cubic structure) was used as calibration data. The measurements were conducted ex-situ at the surface of the coatings which have been subjected to the tribological tests under elevated temperatures. The obtained raw data (XANES spectra) was extracted using the Software PyMca [34] of the European Synchrotron Radiation Facility. To examine the features of the XANES spectra, the data was normalized via standard edge-step normalization, i.e., reduced by background subtraction with a linear function. The absolute energy zero point was chosen in relation to the first inflection point of the V metal derivative spectrum (called E_0), which corresponds to the convection of the excitation of an inner shell electron to an empty state just above the Fermi edge of the V metal. The V foil was scanned to correct the energy shift and to obtain energy-calibrated spectra in a consistent manner. To investigate the specific XANES features, the program package Athena (Demeter Bruce Ravel's XAS Data Analysis Software [35]) was employed. In essence, the absorption edge was taken as the energy of the first point of inflection of the principal absorption edge (given by the maximum in the derivative spectrum), which can be assigned to the energy half way up the normalized-edge step, i.e., where the absorption is equal to 0.5 ($E_{1/2}$). In terms of the pre-edge feature, the data several electronvolts before and after the pre-edge feature was extracted separately, and then fitted with a pseudo-Voigt function as demonstrated in [36]. Afterwards, the pre-edge feature was scrutinized by calculating the pre-edge peak centroid position, pre-edge peak area, and pre-edge peak intensity using the data analysis and graphing software OriginPro as described above.

3. Results and Discussion

3.1. Tribological Investigation

Prior to the tribological examination, the samples used were initially investigated by means of electron microscopy in order to ensure functional integrity. SEM images showing the cross section confirm that the coating consists of a dense and almost defect-free microstructure with no delamination or cracks (see Supplementary Materials, Figure S1). With regard to the chemical composition, EDX analyses confirm that the produced Fe-V coating consists of 55.6 ± 1.2 wt % of Fe, 26.4 ± 0.5 wt % of V, and 15.2 ± 1.0 wt % of O (other bal. wt %). In this respect, the Fe-V coating is interstratified with oxides between individual lamellae. Macroscopically, the arc sprayed Fe-V coating possesses a lamellar microstructure, whereby the individual lamellae exhibit a slight different chemical composition with varying thicknesses. In terms of the oxide formation, XRD analysis [29] verified that the Fe-V coating is mainly composed of V_2O_3, VO and Fe_3O_4. Nevertheless, it is stated that not all phases were identified, since phase transformation processes result in a wide varying non-equilibrium state due to constitutional supercooling during rapid solidification. In addition, the crystallographic data of many metastable phases are not present in the databases.

Figure 1 shows the COF of the arc sprayed Fe-V coating which was obtained from the tribological testing at various temperatures. The V-free steel coating serves as reference. The COF of the Fe-V coating slightly but constantly falls between 25 and 550 °C from 0.66 ± 0.15 to 0.55 ± 0.09. A significant decrease of the COF is observed between 550 and 650 °C (0.55 ± 0.09 → 0.36 ± 0.07). When the sample is exposed to a temperature of 750 °C, the COF further decreases to 0.29 ± 0.05. Opposed to that, the V-free reference exhibits an almost constant COF up to 750 °C of approximately 0.50 ± 0.07. The findings indicate a distinct reduced COF for the Fe-V coating above 550 °C, especially at 750 °C. At 750 °C and under same environmental conditions, the Fe-V coating exhibits a friction reduction of approximately 42% in contrast to the V-free reference. At the same time, the COF decreases by 56% when compared to 25 °C.

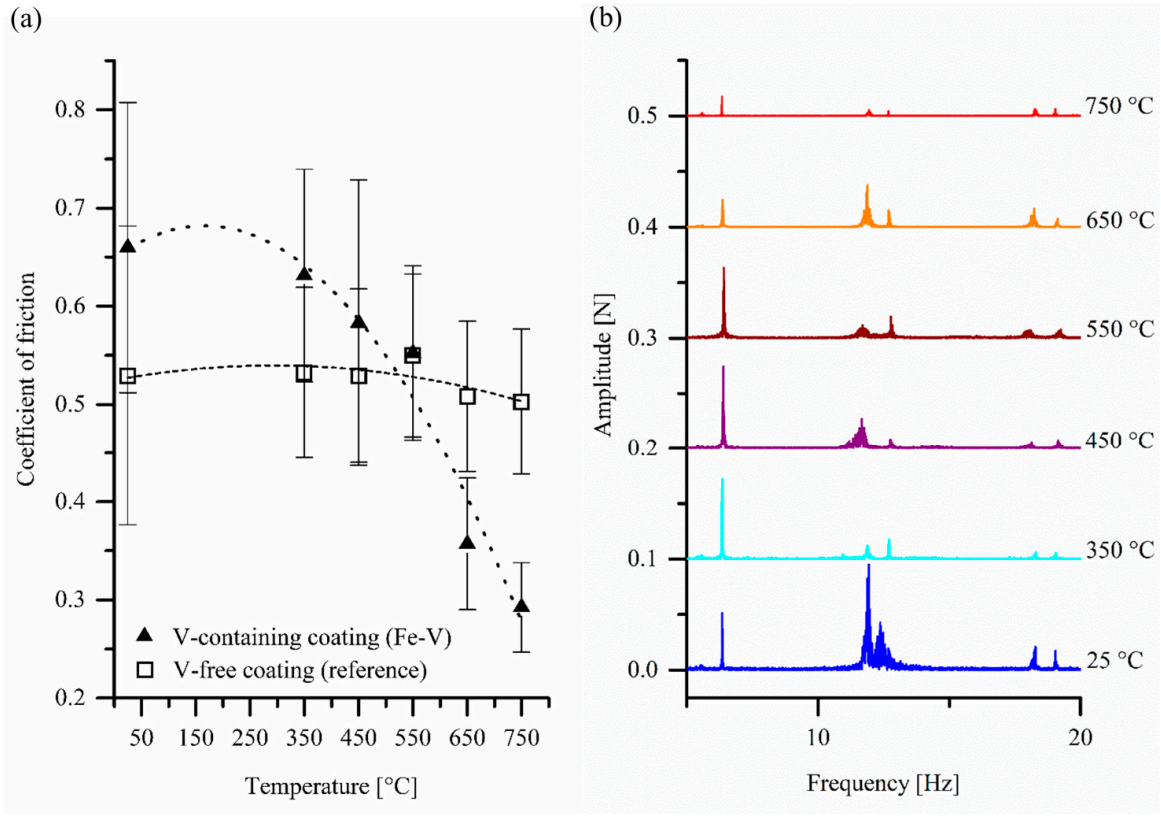

Figure 1. (**a**) Coefficient of friction in dependency on the operating temperature, and (**b**) frequency of the amplitude spectrum calculated from the extracted data of the tangential force measurement during sliding in dependency on the operating temperature.

Stacked FFT analyses of the measured amplitude spectrum revealed that no additional frequencies occurred when the tribological stressed surfaces were subjected to different operating temperatures (Figure 1b). The amplitude expresses the oscillation of the friction forces around the steady state as described in [37]. The spectrum of the amplitude of the coatings is the same for all analyzed temperatures. However, it is striking that the magnitude of the amplitude observed for different temperatures differs distinctly. For instance, at 25 °C the amplitude of the tangential force reaches the highest value, whereas the measurement of the surface which was tribological stressed at 750 °C shows the lowest value. Between the aforementioned temperatures, the amplitude of the friction processes reveals no continuous change with increasing temperature. The findings encourage the assumption that the tribological stressed surface progresses a more constant sliding at elevated temperature, in particular at 750 °C. Reduction of the amplitude is also reported for CrV(x)N thin films for the increase of the temperature from 25 to 550 °C.

The worn surfaces were examined after the tribological tests by means of electron microscopy and EDX spectroscopy (Figure 2). Since the backscattered electrons (BSE) signal is related to the atomic number, an amendment in chemical composition can be obtained. As seen from the SEM images (Figure 2a), mild oxidational regimes are observed across the tribological stressed contact area which was tested at ambient air without any heat treatment. As indicated by electron microscopy, the oxides are mainly formed at cavities, and also in areas of surface disruption which results in certain breakouts of particles. At elevated temperatures up to 450 °C, the Fe-V coating exhibits a tribo-oxidatively formed thin film which can be seen across the wear track. The BSE signal confirms a different chemical composition between the wear track and the surrounding surface area. EDX analyses (Figure 2b) verify an increased amount of oxides across the wear track, when compared to the surrounded surface area. Starting with 550 °C, SEM images show the appearance of oxide grains covering a large part of the surface. At 650 and 750 °C, the surfaces are prone to form various mixed oxides consisting

of different proportions of Fe and V covering the entire surface. As obtained from the BSE signal, the wear track and enclosed surface area exhibit a similar chemical composition. A similar distribution of elements is additionally confirmed by EDX spot analyses. For the tribological stressed surface at 750 °C, EDX analyses reveal that both the surface oxidation and tribo-oxidation is amplified. Thus, it can be concluded that above 450 °C the amount of oxides on the coating surface is significantly higher compared to 25 °C (Figure 2b).

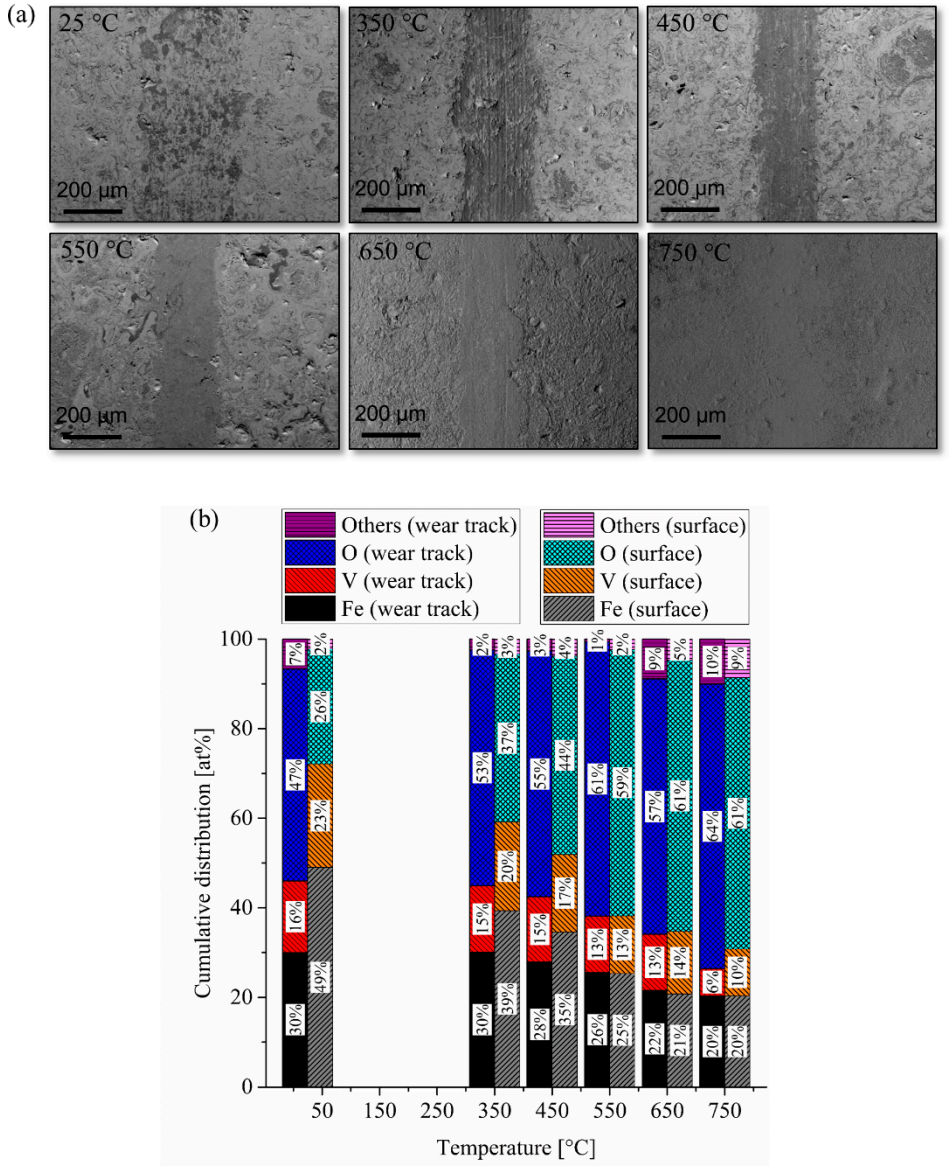

Figure 2. (**a**) SEM images showing the wear tracks after tribological testing, and (**b**) distribution of elements determined by EDX in at % at different spots in dependency of the operating temperature during tribological testing.

Figure 3 shows a magnified view of the wear tracks after sliding at 550, 650 and 750 °C as well as the corresponding SEM images which were detected by the BSE and secondary electrons (SE) signal. With regard to the tribological stressed surface which has been exposed to a temperature of 550 °C during testing, it can be seen that the contact zone predominantly exhibits a covering oxide film (Figure 3, BSE-mode at 550 °C). Individual areas in turn show a local surface disruption (Figure 3, SE-mode at 550 °C).

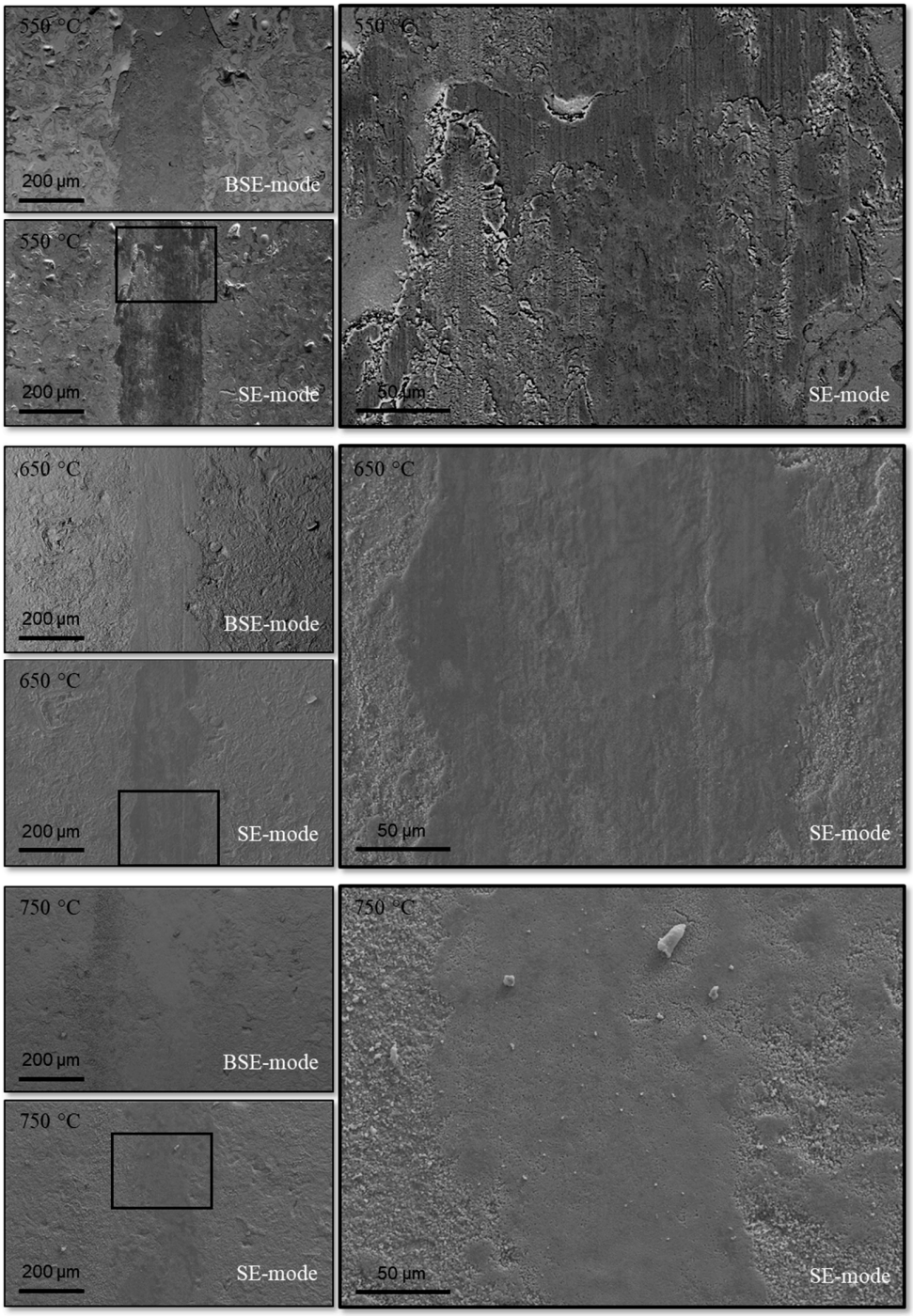

Figure 3. SEM images showing the wear tracks after tribological testing at 550, 650 and 750 °C, using different contrasting methods as well as in a magnified view.

A number of small grooves in the direction of sliding are visible in a magnified view. It is stated the torn out wear particles have been sliding between the two sliding surfaces, and thus, dragging across the softer Fe-V coating. As a result, the wear particles which are ploughing through the Fe-V coating remove the material and cause abrasion such as grooves, indicating three-body wear [38].

For the tribological stressed surface at 650 °C, the material is smeared in the direction of sliding (Figure 3, SE-mode at 650 °C). Shear tongues are formed and a slight amount is drawn out in the direction of sliding. At 750 °C, the coating surface exhibits no significant material removal. In contrast, it can be seen that oxide grains are smoothened and compacted (Figure 3, SE-mode at 750 °C).

A so-called "glaze" is formed at the contact area which was running against the alumina counterbody. It is assumed that the glaze is formed from sintered wear particles such as oxide grains.

Figure 4 shows the wear flat on the alumina counterbody after sliding against the coated sample at 550, 650, and 750 °C. As shown in the SEM images, the alumina counterbodies are hardly abraded. Substantially, material accumulation at the wear flat on the alumina counterbody shows an adhesive wear. However, the counterbodies examined at different temperatures show a different extent of wear. Concerning the examinations above 25 °C, it is found that with increasing temperature a larger amount of material adheres onto the wear flat of the alumina counterbody. Such adhesion is more pronounced at 550 °C when compared to 25, 350 or 450 °C (data not shown). Above 550 °C (650 °C → 750 °C), a distinctly increased amount of material adheres onto the wear flat of the alumina counterbody. In addition, that material is strongly smeared and elongated in the sliding direction. A comparison between the different counterbodies shows that for the counterbody, which was sliding against the coating at 750 °C, the smeared material is much more elongated in the sliding direction. For the adhered material observed at various temperatures, EDX analyses confirm that the material is composed of V-(Fe-) rich oxides. However, as demonstrated in Figure 4, EDX spot analyses (see Spectrum 1, 3 and 5) verify an increased V content in the adhered material, in particular after the dry sliding experiments at 650 and 750 °C. Since it can be assumed that the alumina counterbody is chemically inert, the Al content in the region of the adhered material (Spectrum 1, 3 and 5) can be explained by the inherent characteristics of the EDX spectroscopy, i.e., the interaction between the primary electron beam and the alumina (EDX spot analyses were carried out with 20 keV). According to the findings, it can be concluded that a certain amount of the material originated from the tribological stressed surface adheres on the alumina counterbody.

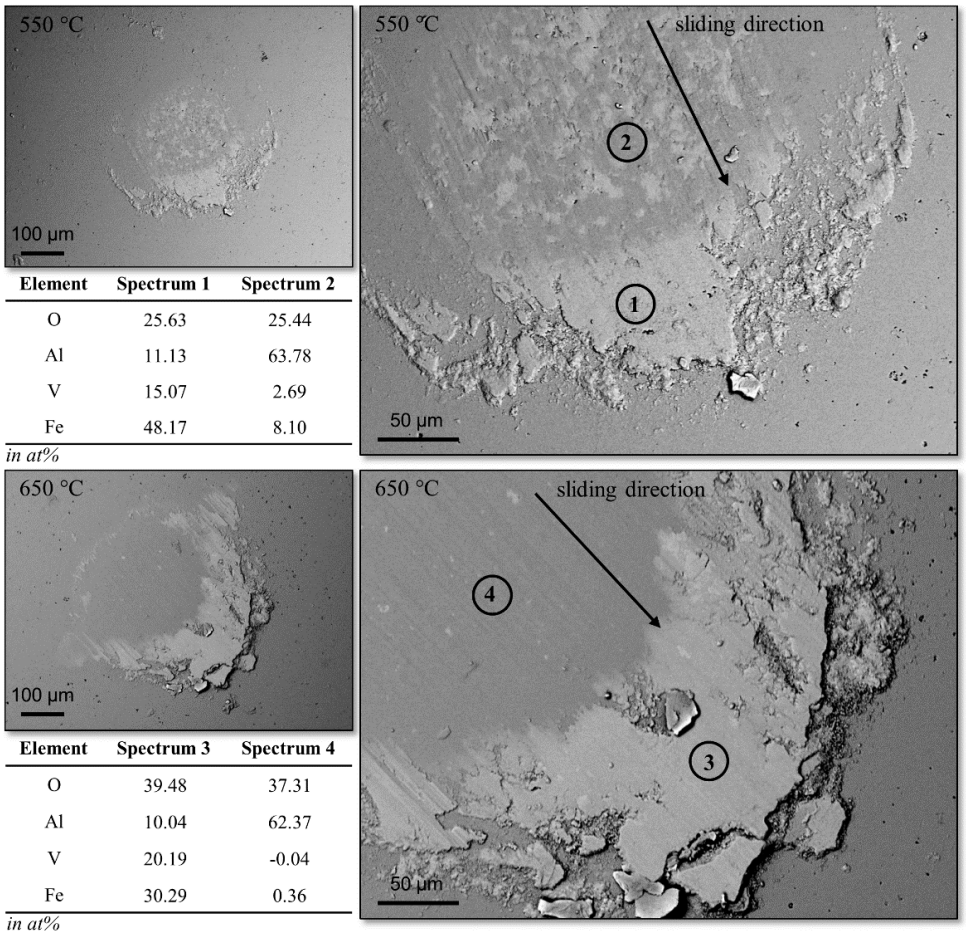

Element	Spectrum 1	Spectrum 2
O	25.63	25.44
Al	11.13	63.78
V	15.07	2.69
Fe	48.17	8.10

in at%

Element	Spectrum 3	Spectrum 4
O	39.48	37.31
Al	10.04	62.37
V	20.19	-0.04
Fe	30.29	0.36

in at%

Figure 4. *Cont.*

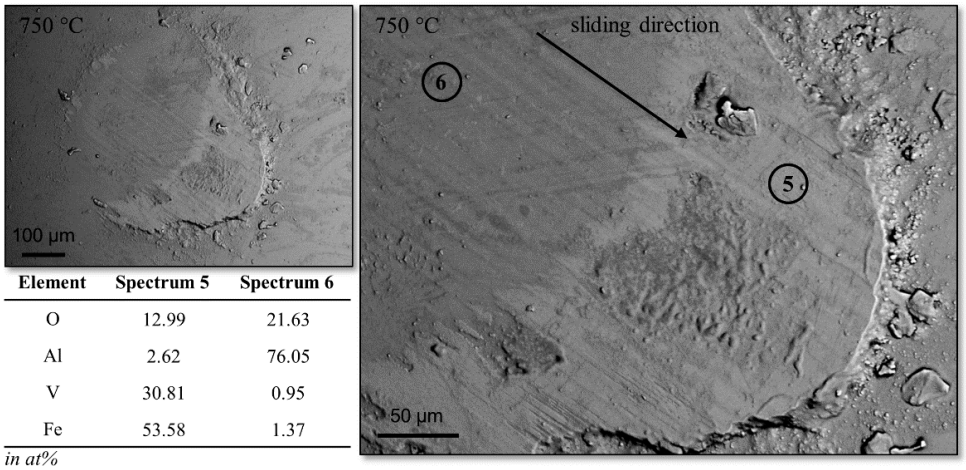

Element	Spectrum 5	Spectrum 6
O	12.99	21.63
Al	2.62	76.05
V	30.81	0.95
Fe	53.58	1.37

in at%

Figure 4. SEM images showing the wear flat on the alumina counterbody after sliding against the coated sample depending on the operating temperature. For the marked regions (Spectrums 1 to 6), the chemical composition is determined by means of EDX.

3.2. XANES Spectroscopy

In order to constrain the average V oxidation state of the coatings, XANES spectra at the V K-edge of several references (vanadium oxides, metallic vanadium), which corresponds to different valence states, were initially measured. The phase purity for V_2O_5 and V_2O_3 was confirmed by XRD. The measurements indicate that the V_2O_5 (V^{5+}) features an orthorhombic crystalline structure, whereas the V_2O_3 (V^{3+}) exists in a trigonal crystalline structure. Further analyses of the other reference oxides confirm no phase purity. VO (V^{2+}) exists as the cubic phase, and includes also the monoclinic V_2O_4 phase. V_2O_4 (V^{4+}) consists mainly of the tetragonal phase, whereby it also includes some amount of the orthorhombic and monoclinic phase as well as orthorhombic V_2O_5. The V_6O_{13} ($V^{4.3+}$) reference features a monoclinic crystalline structure with some traces of V_2O_3 and V_2O_5. Normalized XANES spectra for the references investigated in this study, i.e., various V oxides, are shown in Figure 5a.

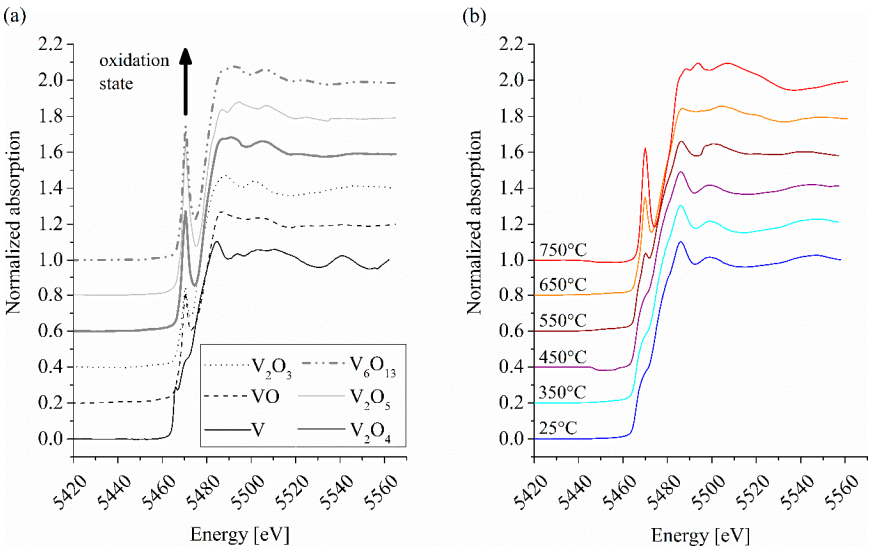

Figure 5. XANES spectra at the V K-edge of (**a**) several vanadium oxides and metallic vanadium, as well as (**b**) XANES spectra at the V K-edge of the coating surface for various temperatures.

Evaluating the different XANES spectra, it is found that the spectra demonstrate significant variations in certain features such as the energy position and intensity of the peaks in the pre-edge region as well as in the edge region. With respect to the absorption edge position, it is shown the

edge energy $E_{1/2}$ of the references (Figure 5a, Table 1) demonstrates a shift to higher energies with increase in the oxidation state of V. For instance, the energy position of the absorption edge tends to rise from 8.7 eV after the K-edge for V^{2+} to 13.8 eV for V^{5+}. The energy shifts are assigned to Kunzl's law as shown in [39], which states that as the valence of the central absorbing atom (i.e., absorbing V atom) increases, all absorption features shift towards higher energy. It needs to be mentioned that the energy shift follows Kunzl's law when a comparison is made among compounds with the same metal-ligand combinations. However, the unambiguous determination of the valence states with the help of the Kunzl's law for some cases is difficult, since the ranges of the chemical shift for two different valences can sometimes overlap. Chaurand et al. [40] pointed out that shape of the XANES spectra at the absorption edge is quite sensitive to the valence state. However, they also reported that the features at the absorption edge are susceptible to the local atomic surrounding, or to a range of interferences such as multiscattering effects arising from more distant neighbors around the central V atoms. Several vanadium oxides, showing an oxidation state from 0 to 5, were analyzed by means of XANES spectroscopy. As obtained from the normalized XANES spectra, the pre-edge peak features of references show distinct variations as well (Figure 5a, Table 1). The V-foil exhibits a pre-edge peak at a centroid position of 5466 eV. Additionally, a subsequent shoulder at 5471 eV is observed before the absorption increases. Opposed to that, the V oxides are characterized by a pre-edge peak centroid position at 5470.5 eV indicating an amendment of the oxidation state or symmetry. The intensity of the pre-edge maximum increases from 0.29 for V to 0.85 for V_2O_5, which corresponds with the chemical alteration (i.e., oxidation state) of V, as shown in Table 1.

Table 1. Characteristic XANES features of the vanadium oxides and metallic vanadium.

Phase	Oxidation-State	Pre-Edge		Main-Edge Position (eV)
		Normalized Intensity	Position (eV)	
V	0	0.29	1	9.5
VO	2	0.62	5.5	8.7
V_2O_3	3	0.44	5.5	10.8
V_2O_4	4	0.67	5.5	13.2
V_6O_{13}	4.3	0.75	5.5	14.4
V_2O_5	5	0.85	5.5	13.8

According to Rees et al. [41], the pre-edge feature is related to electronic transitions from the 1s core levels to the empty 3d levels. As discussed in [42], the transition is induced due to the mixing of 3d orbitals of vanadium with 2p orbitals of oxygen. Studying the speciation of V in oxide phases from steel slag, Chaurand et al. [40] concluded that V^{3+} compounds could be assigned to a pre-edge peak intensity of 0.05–0.10, whereas V^{4+} compounds and V^{5+} compounds could be linked to an intensity of 0.30–0.65 and 0.50–1.20, respectively, depending on the local symmetry. In this respect, V-oxides which consist of a tetrahedral or pyramidal symmetry were characterized by a more intense pre-edge maximum when compared to an octahedral symmetry [40,43]. The authors claimed that the intensity gets influenced, inter alia, by diverse energy resolution by using different monochromator reflections. As a result, the pre-edge peak intensity allows an insufficient discrimination of the vanadium valence. Quoting their discussion on different methodologies examining the pre-edge features [39,44–49], Chaurand et al. [40] in turn clarified that the correlation between the pre-edge peak centroid position and its integrated area represents the most reliable method for determining the speciation of V. Thus, substantial changes occur in both the energy position (i.e., centroid position) and total area of the pre-edge peak.

The normalized XANES spectra measured at the not worn surface of the arc sprayed Fe-V coatings after tribological testing at different temperatures are illustrated in Figure 5b. The characteristic features obtained from the XANES spectra (i.e., normalized pre-edge maximum intensity, centroid position, and main edge position) are summarized in Table 2.

Table 2. Characteristic XANES features of the arc sprayed V-containing Fe-based coating after tribological testing at different temperatures.

Coating Temperature (°C)	Pre-Edge		Main-Edge Position (eV)
	Normalized Intensity	Position (eV)	
25	0.39 *	5 *	9.5
350	0.39 *	5 *	9.5
450	0.43 *	5 *	9.5
550	0.47	5	9.8
650	0.57	5	11.6
750	0.74	5	12.5

The absorption at 25, 350 and 450 °C runs a similar course and shows no pronounced pre-edge peak (marked with * in Table 2), which in turn indicate no distinct oxidation. Starting from 550 °C, a pre-edge peak is gradually formed, that is more intense at 650 and 750 °C. Furthermore, for the same temperature increase (550 °C → 750 °C), the absorption edge shifts to higher energies suggesting an onset of oxidation. In terms of the near-edge structure above the onset of the absorption edge, the different form of oscillation indicates the emergence of new phases with higher oxidation states and different local symmetry. As verified by Farges [50], those features at the absorption edge are predominantly sensitive to the valence and local atomic surrounding of the absorbing element. However, as reported by the same author, the features are also influenced by single or multiple scattering effects as well as changes in the medium and long range environment.

In the next step, we investigate the correlation between the normalized pre-edge peak area and the pre-edge centroid position of the treated Fe-V coatings as well as of the vanadium oxides (Figure 6).

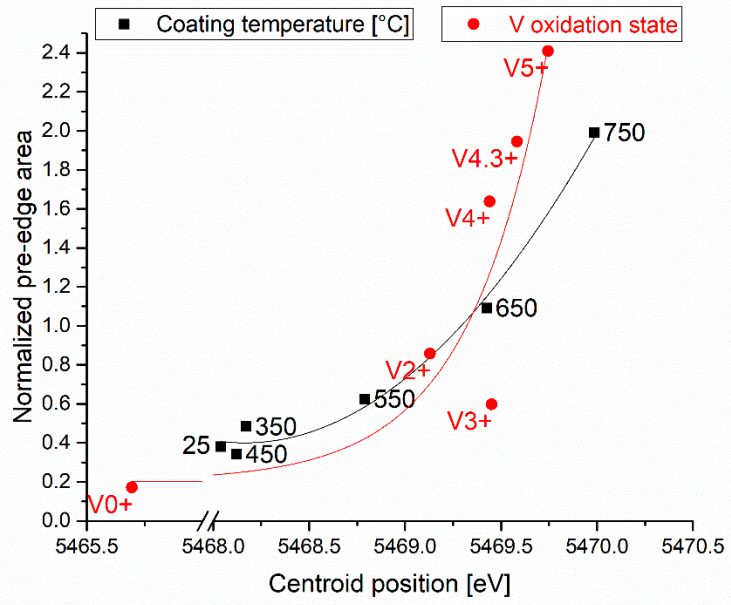

Figure 6. Dependence of pre-edge maximum centroid position and pre-edge maximum area of different treated Fe-V coatings and vanadium oxides (references).

It is found that both the pre-edge peak centroid position and the normalized area of the corresponding peak increase with a larger oxidation state of V. Whereas the normalized pre-edge peak area of pure V is small, a strong increase occurs with rising oxidation state. Since the centroid position and normalized area of the pre-edge peak depend on the crystal structure, the irregularity between V^{2+} and V^{3+} can be attributed to the impurity of references owing to a mixture of different vanadium oxides. For a temperature of 25 °C, the Fe-V coating reveals a pre-edge peak centroid position of 5468.0 eV and a normalized area of 0.38, which corresponds to an oxidation state higher than V^{0+} and

lower than V^{2+}, or V^{3+} respectively. XRD analysis of the as-sprayed coating reveals the occurrence of V_2O_3 and VO as reported in a previous study [29]. Since the oxidation state of VO and V_2O_3 is 2 respectively 3, the position of the pre-edge peak obtained by the XANES spectra illustrates that the coating is not fully oxidized and contains un-oxidized vanadium. Accordingly, the Fe-V coating in its initially state (i.e., as-sprayed and polished conditions) is already interstratified with V-rich oxides which is due to the use of compressed air as atomization gas as well as the environmental conditions during spraying in ambient air. A heat treatment of the Fe-V coating at 350 and 450 °C shows no considerable influence on the pre-edge peak characteristics. Correspondingly, no change in the phase composition is obtained by means of XRD. Hence, the heat treatment at 350 and 450 °C in ambient air does not influence the oxidation state of the V component as measured at the coating surface. The slight increase in surface oxidation up to 450 °C (see EDX, Figure 2b) may be traced back to the formation of Fe-rich oxides. This in turn corresponds to the BSE signal as demonstrated in Figure 2a, indicating some amplified tribo-oxidation phenomena at the wear track with the participation of Fe-rich oxides. In contrast, an increased temperature of 550 °C reveals an amendment of the oxidation state between V^{2+} and V^{3+} as shown by a pre-edge peak centroid position of 5468.8 eV with a normalized pre-edge peak area of 0.62. According to the XRD analyses, due to the heat treatment at 550, 650 and 750 °C the formation of VO_2 and V_2O_5 as well as ternary oxides of the Fe-V-O system takes place [29]. However, the analysis of the XRD patterns is not distinct since a superposition of the reflections of miscellaneous oxides is present. Accordingly, XANES spectroscopy can be used to estimate the average oxidation state of the coatings at different temperatures. For a temperature of 650 °C, a pre-edge peak centroid position of 5469.4 eV and a normalized pre-edge peak area of 1.09 are calculated. Compared to the reference oxides, the determined pre-edge peak characteristics reveal an oxidation state between V^{3+} and V^{4+}. As verified by the SEM images, the coating surface is subjected to a significant oxidation. A further increase in temperature up to 750 °C causes an ongoing oxidation process to an oxidation state between $V^{4.3+}$ and V^{5+} as shown by a pre-edge peak centroid position of 5470.0 eV and normalized pre-edge peak area of 1.99. Comparing both the fit of the reference oxides depending on the oxidation state and the fit of the heat treated Fe-V coating at different temperatures (Figure 6), it is to state that the general pathway of the two fits differs. In fact, the references (Figure 5a) consist of compounds of the binary V–O system, whereas the formation of miscellaneous oxides related to the Fe–V–O system or other phases of the Fe–V system on the coating surface (Figure 5b) could not be ruled out. Accordingly, the scattering of the radiation on other atoms, such as Fe, can affect the absorption and consequently the position and shape of the peaks [51]. However, it can be concluded that the oxidation state of the V component, as detected on the surface of the Fe–V coating, increases with increasing temperature. Similar findings were observed studying the oxidation behavior of $AlCrV_xN$ thin films at various temperatures [24]. With respect to the tribological investigations (Figure 1), it is found that the COF initially drops gradually until a temperature of 450 °C, which then decreases significantly with increasing temperature starting from 550 °C. Since the oxidation state of the V component increases above 450 °C, it is believed that the oxidation state of the V component in the reactive layer has a fundamental impact on the resulting friction behavior (i.e., the alumina counterbody has a high chemical inertness). Quoting the discussion on various studies on V-containing hard coatings, the authors recently clarified in [24] that the reduction of the COF is attributed, among others, to the formation of certain Magnéli phases. Despite a ferrovanadium alloy as feedstock, the oxidation of vanadium is fostered at elevated temperature, leading to a possible formation of self-lubricous vanadium oxides which causes the reduction of the COF. The pre-oxidized state of the Fe-V coating under as-sprayed conditions does not influence the ongoing oxidation process at elevated temperatures.

4. Conclusions

A vanadium-containing iron-based coating was deposited by means of arc spraying with a resulting vanadium content of up to 26.4 ± 0.5 wt %. As verified in dry sliding experiments,

the COF of the vanadium-containing coating decreases gradually until reaching a temperature of 450 °C. With further increases in temperature starting from 550 °C the COF drops significantly. In contrast, a vanadium-free reference features an almost constant COF up to 750 °C. Evaluating the dry sliding behavior under same environmental conditions, i.e., at a temperature of 750 °C, the vanadium-containing coating possesses a friction reduction of approximately 42% compared to the vanadium free reference. Simultaneously, the COF decreases by 56% when compared to 25 °C. As confirmed by certain pre-edge peak characteristics using XANES spectroscopy, the reduction of friction starting from 550 °C corresponds with an average oxidation state higher than V2+. Further surface oxidation phenomena at 650 and 750 °C, respectively, are attributed to a further increased oxidation state for the V component.

Supplementary Materials: The following are available online at http://www.mdpi.com/2079-6412/9/1/18/s1, Figure S1: SEM image showing the cross section of the produced V-containing Fe-based coating.

Author Contributions: Conceptualization, L.H.; Investigation, L.H., D.K. and M.P.; Writing-Original Draft Preparation, L.H., D.K. and M.P.; Writing-Review & Editing, L.H. and D.K.; Supervision, W.T. and M.T.; Project Administration, L.H.

Funding: This research received no external funding.

Acknowledgments: The contributions of DURUM Verschleissschutz GmbH are gratefully acknowledged for their support in providing the vanadium-containing feedstock. The authors would like to thank the DELTA machine group for providing synchrotron radiation.

Conflicts of Interest: The authors declare no conflict of interest.

References

1. Woydt, M.; Skopp, A.; Dörfel, I.; Witke, K. Wear Engineering Oxides/Antiwear Oxides©. *Tribol. Trans.* **1999**, *42*, 21–31. [CrossRef]
2. Franz, R.; Mitterer, C. Vanadium containing self-adaptive low-friction hard coatings for high-temperature applications: A review. *Surf. Coat. Technol.* **2013**, *228*, 1–13. [CrossRef]
3. Brugnara, R.H. Hochtemperaturaktive HPPMS-Verschleißschutzschichten durch Bildung reibmindernder Magnéli-Phasen im System (Cr,Al,X)N. Ph.D. Thesis, Technische Hochschule Aachen, Aachen, Germany, January 2016. (In German)
4. Stegemann, B.; Klemm, M.; Horn, S.; Woydt, M. Switching adhesion forces bycrossing the metal-insulator transition in Magneli-type vanadium oxide crystals. *Beilstein J. Nanotechnol.* **2011**, *2*, 59–65. [CrossRef] [PubMed]
5. Reeswinkel, T.; Music, D.; Schneider, J.M. Ab initio calculations of the structure and mechanical properties of vanadium oxides. *J. Phys. Condens. Matter* **2009**, *21*, 145404. [PubMed]
6. Lamsal, C.; Ravindra, N.M. Optical properties of vanadium oxides-an analysis. *J. Mater. Sci.* **2013**, *48*, 6341–6351. [CrossRef]
7. Hryha, E.; Rutqvist, E.; Nyborg, L. Stoichiometric vanadium oxides studied by XPS. *Surf. Interface Anal.* **2012**, *44*, 1022–1025. [CrossRef]
8. Kharton, V. *Solid State Electrochemistry I: Fundamentals, Materials and their Applications*; John Wiley & Sons: Weinheim, Germany, 2009.
9. Woydt, M.; Skopp, A.; Dörfel, I.; Witke, K. Wear engineering oxides/anti-wear oxides. *Wear* **1998**, *218*, 84–95.
10. Lugscheider, E.; Bärwulf, S.; Barimani, C. Properties of tungsten and vanadium oxides deposited by MSIP-PVD process for self-lubricating applications. *Surf. Coat. Technol.* **1999**, *120–121*, 458–464. [CrossRef]
11. Lugscheider, E.; Knotek, O.; Bobzin, K.; Bärwulf, S. Tribological properties, phase generation and high temperature phase stability of tungsten- and vanadium-oxides deposited by reactive MSIP-PVD process for innovative lubrication applications. *Surf. Coat. Technol.* **2000**, *133–134*, 362–368. [CrossRef]
12. Gulbiński, W.; Suszko, T.; Sienicki, W.; Warcholiński, B. Tribological properties of silver- and copper-doped transition metal oxide coatings. *Wear* **2003**, *254*, 129–135. [CrossRef]
13. Vernardou, D.; Louloudakis, D.; Spanakis, E.; Katsarakis, N.; Koudoumas, E. Electrochemical properties of vanadium oxide coatings grown by hydrothermal synthesis on FTO substrates. *New J. Chem.* **2014**, *38*, 1959–1964. [CrossRef]

14. Louloudakis, D.; Vernardou, D.; Spanakis, E.; Katsarakis, N.; Koudoumas, E. Electrochemical properties of vanadium oxide coatings grown by APCVD on glass substrates. *Surf. Coat. Technol.* **2013**, *230*, 186–189. [CrossRef]
15. Qui, Y.; Zhang, S.; Lee, J.W.; Li, B.; Wang, Y.; Zhao, D.; Sun, D. Towards hard yet self-lubricious CrAlSiN coatings. *J. Alloy. Comp.* **2015**, *618*, 132–138.
16. Fernandes, F.; Loureiro, A.; Polcar, T.; Cavaleiro, A. The effect of increasing V content on the structure, mechanical properties and oxidation resistance of Ti-Si-V-N films deposited by DC reactive magnetron sputtering. *Appl. Sur. Sci.* **2014**, *289*, 114–123. [CrossRef]
17. Bobzin, K.; Bagcivan, N.; Ewering, M.; Brugnara, R.H.; Theiss, S. DC-MSIP/HPPMS (Cr,Al,V)N and (Cr,Al,W)N thin films for high-temperature friction reduction. *Surf. Coat. Technol.* **2011**, *205*, 2887–2892. [CrossRef]
18. Franz, R.; Neidhardt, J.; Mitterer, C.; Schaffer, B.; Hutter, H.; Kaindl, R.; Sartory, B.; Tessadri, R.; Lechthaler, M.; Polcik, P. Oxidation and diffusion processes during annealing of AlCrVN hard coatings. *J. Vac. Sci. Technol. A* **2008**, *26*, 302–308. [CrossRef]
19. Chang, Y.Y.; Chiu, W.T.; Hung, J.P. Mechanical properties and high temperature oxidation of CrAlSiN/TiVN hard coatings synthesized by cathodic arc evaporation. *Surf. Coat. Technol.* **2016**, *303 Pt A*, 18–24. [CrossRef]
20. Qiu, Y.; Zhang, S.; Lee, J.W.; Li, B.; Wang, Y.; Zhao, D. Self-lubricating CrAlN/VN multilayer coatings at room temperature. *Appl. Surf. Sci.* **2013**, *279*, 189–196. [CrossRef]
21. Luo, Q. Temperature dependent friction and wear of magnetron sputtered coating TiAlN/VN. *Wear* **2011**, *271*, 2058–2066. [CrossRef]
22. Qui, Y.; Zhang, S.; Li, B.; Wang, Y.; Lee, J.W.; Li, F.; Zhao, D. Improvement of tribological performance of CrN coating via multilayering with VN. *Surf. Coat. Technol.* **2013**, *231*, 357–363.
23. Park, J.K.; Baik, Y.J. Increase of hardness and oxidation resistance of VN coating by nanoscale multilayered structurization with AlN. *Mater. Lett.* **2008**, *62*, 2528–2530. [CrossRef]
24. Tillmann, W.; Kokalj, D.; Stangier, D.; Paulus, M.; Sternemann, C.; Tolan, M. Investigation on the oxidation behavior of $AlCrV_xN$ thin films by means of synchrotron radiation and influence on the high temperature friction. *Appl. Surf. Sci.* **2018**, *427*, 511–521. [CrossRef]
25. Wriedt, H.A. The O–V (Oxygen-Vanadium) system. *Bull. Alloy Phase Diagr.* **1989**, *10*, 271–277. [CrossRef]
26. Kutschej, K.; Mayrhofer, P.H.; Kathrein, M.; Polcik, P.; Mitterer, C. A new low-friction concept for $Ti_{1-x}Al_xN$ based coatings in high-temperature applications. *Surf. Coat. Technol.* **2004**, *188–189*, 358–363. [CrossRef]
27. Deng, Y.; Yu, S.F.; Yan, N.; Xing, S.L.; Huang, L.B. Effect of vanadium and niobium on abrasive behaviour of arc sprayed 4Cr13 coatings. *Appl. Mech. Mater.* **2013**, *395*, 712–717. [CrossRef]
28. PL 40933 EN 07 PPG SmartArc®Gun Parts List (EN). Available online: https://www.oerlikon.com/metco/en/products-services/coating-equipment/thermal-spray/spray-guns/spray-guns-arc/ppg/ (accessed on 27 December 2018).
29. Tillmann, W.; Hagen, L.; Kokalj, D.; Paulus, M.; Tolan, M. A study on the tribological behavior of vanadium-doped arc sprayed coatings. *J. Therm. Spray Technol.* **2017**, *26*, 503–516. [CrossRef]
30. Federation of European Producers of Abrasives. FEPA Grains Standards. Available online: https://www.fepa-abrasives.com/abrasive-products/grains (accessed on 27 December 2018).
31. Newbery, A.P.; Grant, P.S.; Neiser, R.A. The velocity and temperature of steel droplets during electric arc spraying. *Surf. Coat. Technol.* **2005**, *195*, 91–101. [CrossRef]
32. Guo, W.; Wu, Y.; Zhang, J.; Yuan, W. Effect of the long-term heat treatment on the cyclic oxidation behavior of Fe-based amorphous/nanocrystalline coatings prepared by high-velocity arc spray process. *Surf. Coat. Technol.* **2016**, *307*, 392–398. [CrossRef]
33. Cheng, J.; Zhao, S.; Liu, D.; Feng, Y.; Liang, X. Microstructure and fracture toughness of the FePSiB-based amorphous/nanocrystalline coatings. *Mater. Sci. Eng. A* **2017**, *696*, 341–347. [CrossRef]
34. Solé, V.A.; Papillon, E.; Cotte, M.; Walter, P.; Susini, J. A multiplatform code for the analysis of energy-dispersive X-ray fluorescence spectra. *Spectrochim. Acta B* **2007**, *62*, 63–68. [CrossRef]
35. Ravel, B.; Newville, M. ATHENA, ARTEMIS, HEPHAESTUS: Data analysis for X-ray absorption spectroscopy using IFEFFIT. *J. Synchrotron Radiat.* **2005**, *12*, 537–541. [CrossRef] [PubMed]
36. Poumellec, B.; Marucco, J.F.; Touzelin, B. X-ray-absorption near-edge structure of titanium and vanadium in (titanium,vanadium) dioxide rutile solid solutions. *Phys. Rev. B* **1987**, *35*, 2284–2294. [CrossRef]

37. Perfilyev, V.; Moshkovich, A.; Lapsker, I.; Laikhtman, A.; Rapoport, L. The effect of vanadium content and temperature on stick–slip phenomena under friction of CrV(x)N coatings. *Wear* **2013**, *307*, 44–51. [CrossRef]
38. Hutchings, I.; Shipway, P. Wear by hard particles. In *Tribology*, 2nd ed.; Hutchings, I., Shipway, P., Eds.; Butterworth-Heinemann: Oxford, UK, 2017; pp. 165–236.
39. Wong, J.; Lytle, F.W.; Messmer, R.P.; Maylotte, D.H. K−edge absorption spectra of selected vanadium compounds. *Phys. Rev. B* **1984**, *30*, 5596–5610. [CrossRef]
40. Chaurand, P.; Rose, J.; Briois, V.; Salome, M.; Proux, O.; Nassif, V.; Olivi, L.; Susini, J.; Hazemann, J.L.; Bottero, J.Y. New methodological approach for the vanadium K-edge X-ray absorption near-edge structure interpretation: Application to the speciation of vanadium in oxide phases from steel slag. *J. Phys. Chem. B* **2007**, *111*, 5101–5110. [CrossRef] [PubMed]
41. Rees, J.A.; Wandzilak, A.; Maganas, D.; Wurster, N.I.C.; Hugenbruch, S.; Kowalska, J.K.; Pollock, C.J.; Lima, F.A.; Finkelstein, K.D.; DeBeer, S. Experimental and theoretical correlations between vanadium K-edge X-ray absorption and Kβ emission spectra. *J. Biol. Inorg. Chem.* **2016**, *21*, 793–805. [CrossRef]
42. Tanaka, T.; Yamashita, H.; Tsuchitani, R.; Funabiki, T.; Yoshida, S. X-ray absorption (EXAFS/XANES) study of supported vanadium oxide catalysts. Structure of surface vanadium oxide species on silica and (γ-alumina at a low level of vanadium loading. *J. Chem. Soc. Faraday Trans. 1* **1988**, *84*, 2987–2999. [CrossRef]
43. Krause, B.; Darma, S.; Kaufholz, M.; Mangold, S.; Doyle, S.; Ulrich, S.; Leiste, H.; Stuber, M.; Baumbach, T. Composition-dependent structure of polycrystalline magnetron-sputtered V-Al-C-N hard coatings studied by XRD, XPS XANES and EXAFS. *J. Appl. Crystallogr.* **2013**, *46*, 1064–1075. [CrossRef]
44. Giuli, G.; Paris, E.; Mungall, J.; Romano, C.; Dingwell, D. V oxidation state and coordination number in silicate glasses by XAS. *Am. Mineral.* **2004**, *89*, 1640–1646. [CrossRef]
45. Sutton, S.R.; Karner, J.; Papike, J.; Delaney, J.S.; Shearer, C.; Newville, M.; Eng, P.; Rivers, M.; Dyar, M.D. Vanadium K edge XANES of synthetic and natural basaltic glasses and application to microscale oxygen barometry. *Geochim. Cosmochim. Acta* **2005**, *69*, 2333–2348. [CrossRef]
46. Passerini, S.; Smyrl, W.H.; Berrettoni, M.; Tossici, R.; Rosolen, M.; Marassi, R.; Decker, F. XAS and electrochemical characterization of lithium intercalated V_2O_5 xerogels. *Solid State Ion.* **1996**, *90*, 5–14. [CrossRef]
47. Wilke, M.; Farges, F.; Petit, P.E.; Brown, G.E.J.; Martin, F. Oxidation state and coordination of Fe in minerals: An Fe K-XANES spectroscopic study. *Am. Mineral.* **2001**, *86*, 714–730. [CrossRef]
48. Wilke, M.; Partzsch, G.M.; Bernhardt, R.; Lattard, D. Determination of the iron oxidation state in basaltic glasses using XANES at the K-edge. *Chem. Geol.* **2004**, *213*, 71–87. [CrossRef]
49. Petit, P.-E.; Farges, F.; Wilke, M.; Solé, V.A. Determination of the iron oxidation state in Earth materials using XANES pre-edge information. *J. Synchrotron Radiat.* **2001**, *8*, 952–954. [CrossRef]
50. Farges, F. *Ab initio* and experimental pre-edge investigations of the Mn K-edge XANES in oxide-type materials. *Phys. Rev. B* **2005**, *71*, 155109. [CrossRef]
51. Rehr, J.J.; Albers, R.C. Theoretical approaches to x-ray absorption fine structure. *Rev. Mod. Phys.* **2000**, *72*, 621–654. [CrossRef]